Space & Planetary Physics | Lancaster University

A new database of near-Earth solar wind conditions from Cluster 1 and 3, and comparisons with OMNI projected values

Dr Neil C. Rogers
n.rogers1@lancaster.ac.uk

Neil C. Rogers, J. A. Wild, and A. Grocott
Space & Planetary Physics, Lancaster University, UK

1. Introduction

- Many models of the solar wind (SW) drivers of magnetospheric and ionospheric processes rely on measurements near the L_1 Sun-Earth libration point provided by the **NASA OMNI database** [Papitashvili & King, 2020].
- In this project, we aim to quantify the **uncertainty in the timing and evolution of solar wind conditions** between L_1 and the magnetospheric boundary.
- This will help determine the extent to which the apparent **saturation of the cross-polar cap potential** (CPCP) with increasing solar wind driving is due to statistical uncertainties in OMNI data.

Key findings

- We have generated a **23-year database of near-Earth solar wind** measurements from **ESA Cluster** satellites when they are clearly outside the **Bow Shock (BS)**.
- This comprises approx. 600 periods (approx. **5,000 hours**) for which magnetic field and plasma measurements (density, velocity, temperature) are available from both OMNI and Cluster.
- Restricting to locations > 3 Earth radii (R_E) beyond the Bow Shock gives a closer match to OMNI data, perhaps due to less chance of encountering foreshock modifications of the solar wind.
- Cluster-1 flow velocity measurements are biased 10 km s^{-1} lower than OMNI; Cluster-3 flow velocities are more strongly biased at 14 km s^{-1} lower than OMNI.
- Saturation of CPCP occurs to a similar extent, regardless of whether the solar wind driver E_{KL} is measured near-Earth (by Cluster) or near L_1 (by OMNI).

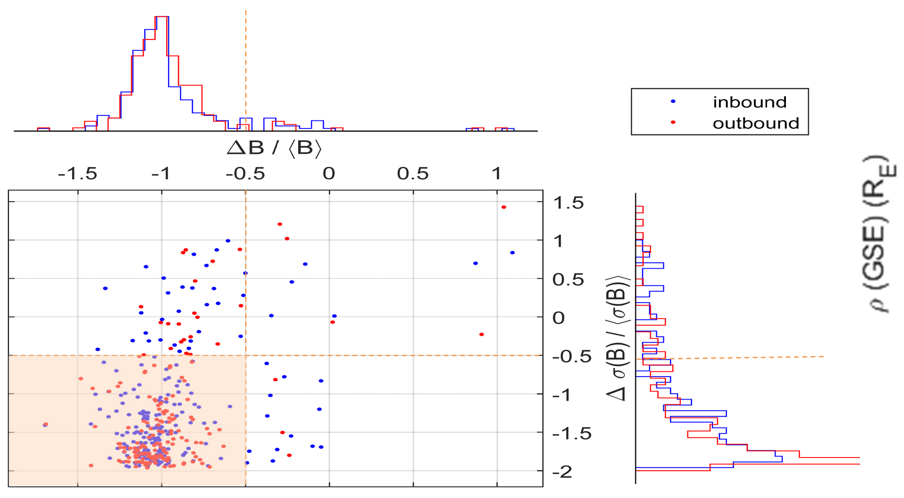

Figure 1: Probability distributions of $\Delta B/\langle B\rangle$ and $\Delta\sigma(B)/\langle\sigma(B)\rangle$ for 10-min windows centred on 403 confirmed BS crossings published by Kruparova et al. [2019]. The orange shaded region is the chosen region of high confidence of BS crossing detection.

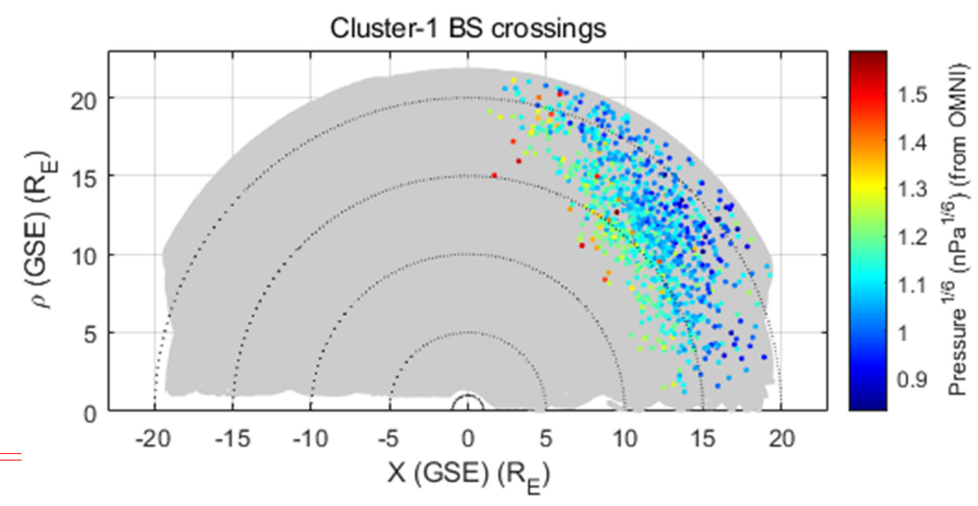

Figure 2. Locations of 1246 Bow Shock crossings for Cluster-1 as a function of distance towards sun (X) and distance from sun-Earth line, ρ. Note how the bow shock location varies with solar wind dynamic pressure, $P^{1/6}$) (colour scale). Grey = all spacecraft locations.

2: Creating a database of near-Earth Solar Wind data

Cluster-1 and -3 measurements were found for periods inside the solar wind using the following method:

- Obtain magnetic Field (***B***) (FGM instrument) and plasma measurements (CIS/HIA instrument) for years 2001-2023.
- Calculate means $\langle\cdot\rangle$ and standard deviations $\sigma(\cdot)$ in each 1-minute period (to match resolution of OMNI dataset).
- Determine Bow Shock crossings based on simultaneous step changes over 10-minute windows with $|\frac{\Delta B}{\langle B\rangle}| > 0.5$, $|\frac{\Delta\sigma(B)}{\sigma(B)}| > 0.5$, and $\Delta B\Delta\sigma(B) > 0$. (These thresholds were determined from analysis of 403 confirmed BS crossings [Kruparova et al., 2019] shown in Figure 1.)
- Retain periods >2 h duration which include apogee.
- Exclude periods with missing data within 30 min of BS crossing.
- Visually inspect auto-detected solar wind periods.
- For plasma measurements: retain periods for which Solar Wind CIS operating modes (0-5) were in operation.

We then optionally exclude periods -

- with CIS/HIA data quality index < 3 (determined by the CIS instrument team),
- where FGM data was subject to caveats, and
- up to 3 R_E (radially) beyond the Bow Shock crossing.

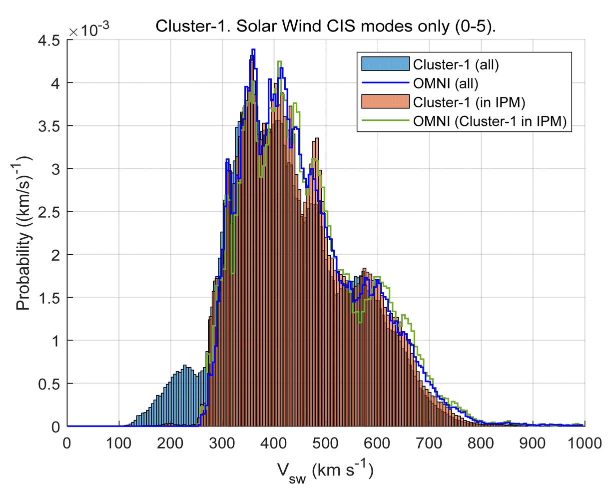

Figure 3. **Blue bars** = Solar wind velocity distribution of all Cluster-1 measurements for CIS modes 0-5 (Solar Wind). **Orange bars** = distribution after BS detection and filters applied. A population of lower velocity (100-270 km s^{-1}) (probably magnetosheath) measurements is removed and the remainder closely match the OMNI velocity distribution (**green line**). (No "back-offs" from BS location are applied)

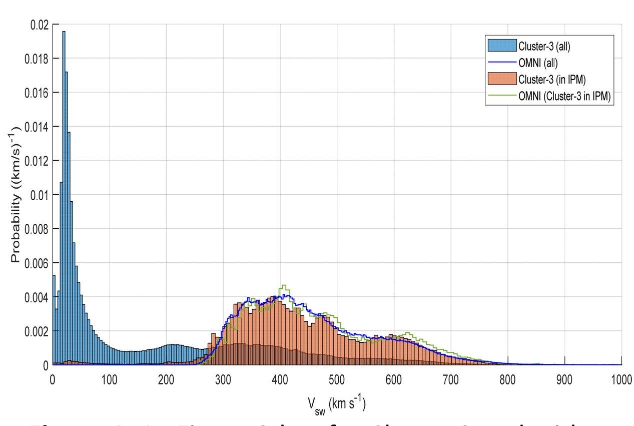

Figure 4. As Figure 3 but for Cluster-3 and with no filtering for CIS operating mode. The "all Cluster" velocity distribution (blue bars) consists mainly of low velocities within the magnetosphere.

3. Comparisons OMNI vs Cluster (inside solar wind)

Figure 5 compares OMNI a) B-field and b) velocity with Cluster-1 measurements inside the solar wind. OMNI velocities are biased 10.0 km s^{-1} higher than Cluster-1 and 13.8 km s^{-1} higher than Cluster-3. Figure 5c shows that Cluster-3 velocities are biased 3.4 km s^{-1} less than Cluster-1.

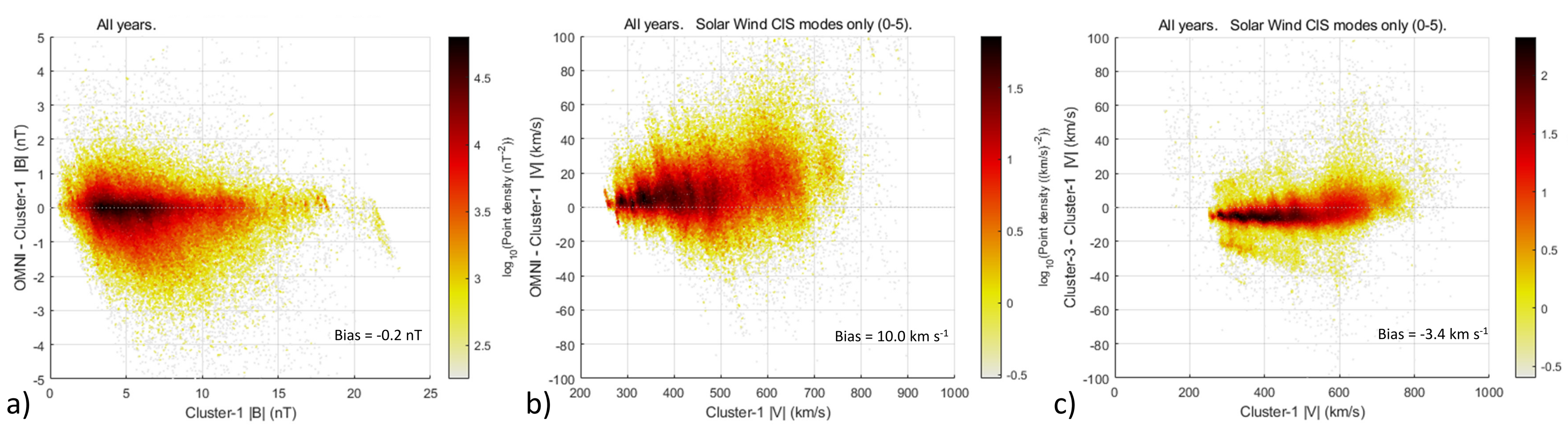

Figure 5. Differences of a) OMNI |B| minus Cluster-1 |B|, b) OMNI |V| minus Cluster-1 |V|, and c) Cluster-3 |V| minus Cluster-1 |V| for periods inside the Solar Wind. Each point represents a 1-min mean. Colours indicate the density of plotted points.

Acknowledgements

- This work is funded by the **UKRI STFC**; Project number ST/Y002040/1.
- We acknowledge the work of the FGM and CIS instrument teams of the ESA Cluster mission and data provided by the Cluster Science Archive (Laakso et al., 2010).
- We acknowledge use of NASA/GSFC's Space Physics Data Facility's OMNIWeb service, and OMNI data.

UKRI Science and Technology Facilities Council

Further filtering may be applied to remove times when Cluster is within 3R_E of the auto-detected BS crossing, and applying a filter based on quality indices published by the CIS instrument team. The effect of this filtering is shown in Figure 6 (below); it removes regions of discrepancy, but also reduces the number of data points.

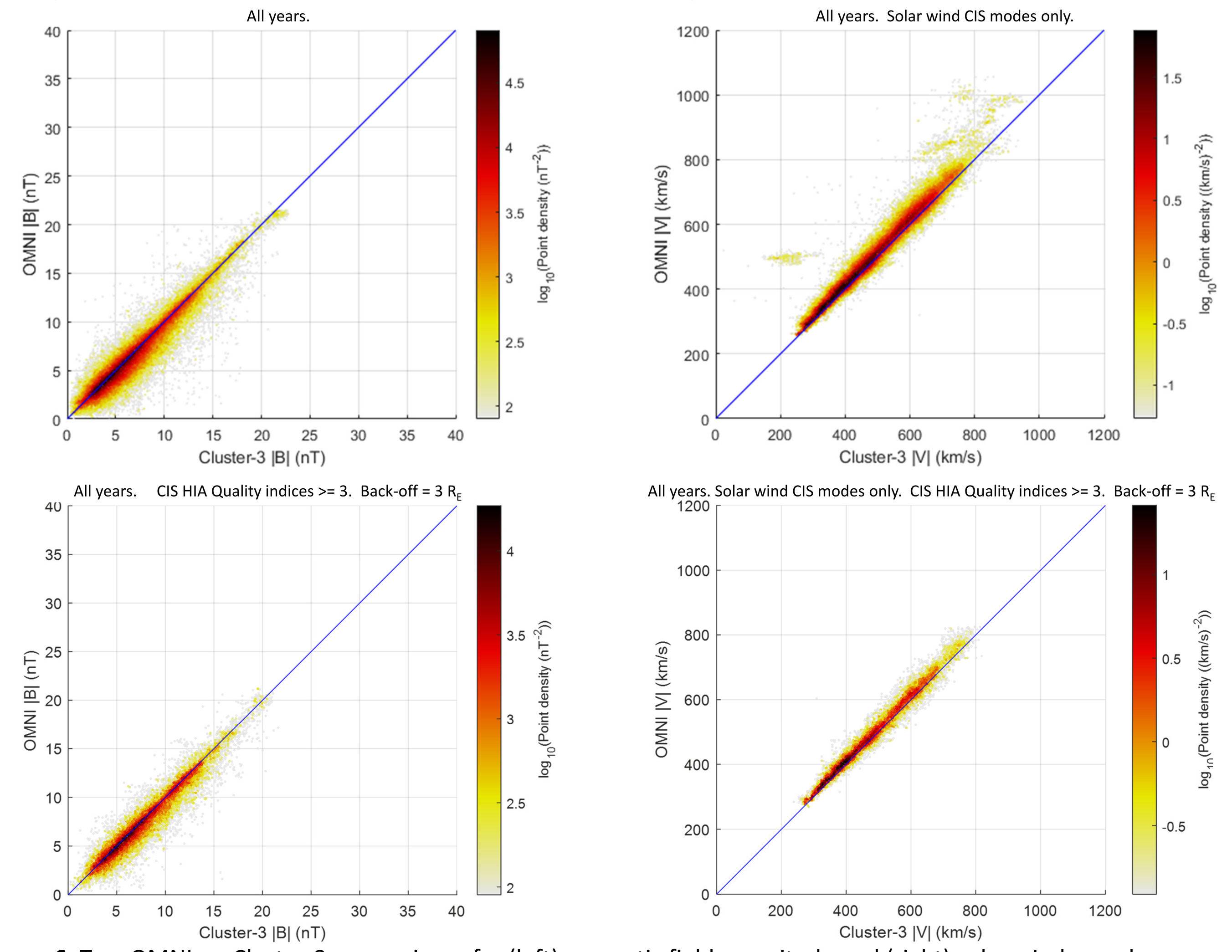

Figure 6. Top: OMNI vs. Cluster-3 comparisons for (left) magnetic field magnitude and (right) solar wind speed. Bottom: The same after excluding measurements within 3 R_E and CIS instrument quality indices < 3.

4. Does uncertainty in the L_1 (OMNI) to near-Earth (Cluster) solar wind projection contribute to the saturation in cross-polar cap potential (CPCP)?

We are addressing this question using our dataset of OMNI (near L_1) and Cluster (near-Earth) solar wind measurements. As a solar wind driver we chose the Kan & Lee (1979) solar wind - magnetosphere coupling function, defined as

$$E_{KL} = |\boldsymbol{V} \times \boldsymbol{B}|\sin^2\left(\frac{\theta_c}{2}\right)$$

where $\boldsymbol{V}$ is the solar wind velocity and, $\theta_c = atan2(B_y, B_z)$ is the 'clock angle' of the magnetic field in GSM coordinates. The ionospheric response, CPCP (or V_{pc}), is determined from SuperDARN maps of ionospheric F-region velocity (from radar Doppler measurements) and a stationary geomagnetic field model.

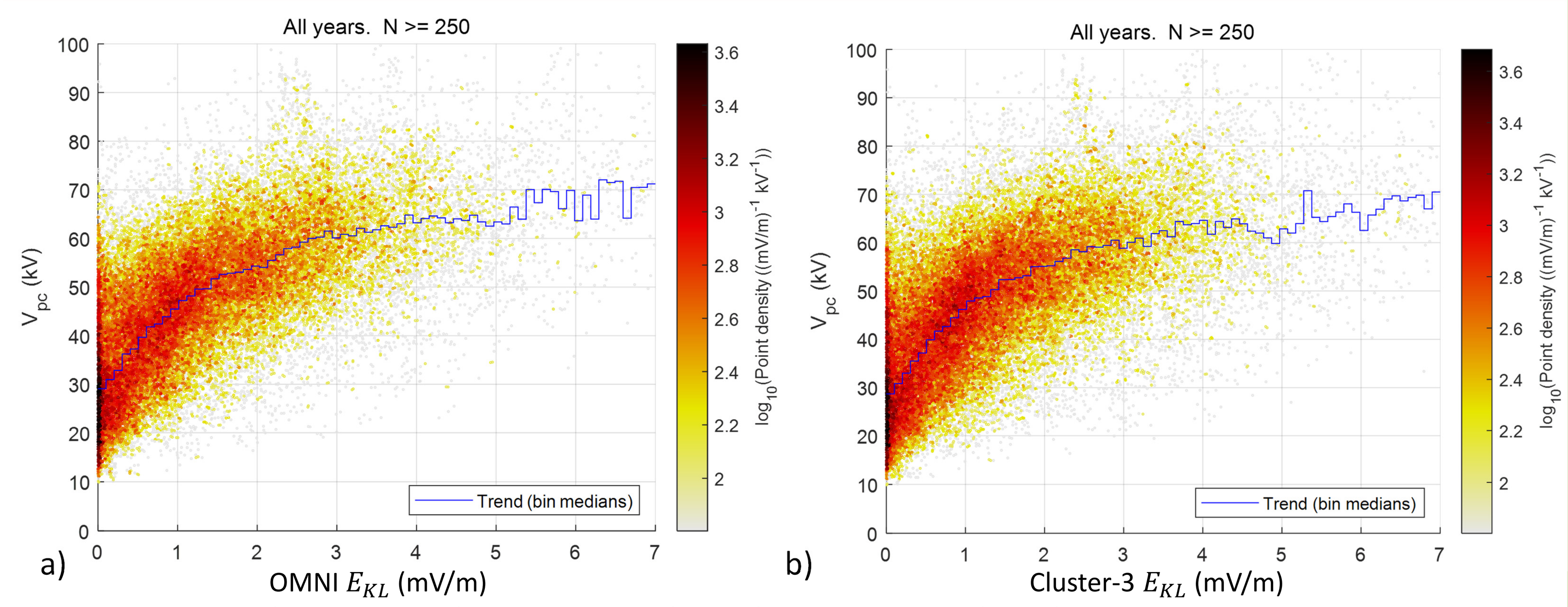

Figure 7. CPCP vs. E_{KL} (solar wind driver) determined from a) OMNI (projected to BS nose) and b) Cluster-3 measurements inside the solar wind. Radar measurements in at least 250 SuperDARN grid cells are required for a valid V_{pc} estimate.

Figure 7 shows that the apparent saturation of the ionospheric response (CPCP) to the solar wind driver E_{KL} is present to a similar extent regardless of whether OMNI or near-Earth solar-wind Cluster data are used.

5. Discussion and Further Work

In the above analysis, we have applied the timing offset of solar wind propagation between the spacecraft near L_1 and a model Bow Shock nose location from the OMNI dataset (typically 30-90 min [Case & Wild, 2012]). We have not yet applied the small adjustments resulting from offsets of the Cluster satellite location relative to the BS nose (+/- 2mins), slowed propagation of the shocked solar wind through the magnetosheath, and the 1-3 min delay between a dayside magnetopause reconnection site and the ionosphere [Khan & Cowley, 1999]. The effect of such timing uncertainties may be lessened by consideration of only steady state solar wind conditions (e.g. following Shepherd et al. 2002).

We will also investigate the effects of instrument measurement accuracy, the impact of 1-min temporal averaging, alternative Solar wind-magnetosphere coupling functions (e.g. Newell et al. 2007), alternative ionospheric responses such as the PC_N index, and the effect of spacecraft distance from the sun-Earth line.

References

- Case, N. A., and J. A. Wild (2012), A statistical comparison of solar wind propagation delays derived from multispacecraft techniques, *J. Geophys. Res.*, *117*, A02101, https://doi.org/10.1029/2011JA016946.
- Laakso, H., *et al.* (Eds.) (2010), Cluster Active Archive: Overview, 3-37, The Cluster Active Archive, *Astrophysics and Space Science Proceedings*, Springer. https://doi.org/10.1007/978-90-481-3499-1_1.
- Kan, J. R., and L. C. Lee (1979) Energy coupling function and solar wind – magnetosphere dynamo, *Geophys. Res. Lett.*, *6*, 577, https://doi.org/10.1029/GL006i007p00577.
- Khan, H., and S. W. H. Cowley (1999), Observations of the response time of high-latitude ionospheric convection to variations in the interplanetary magnetic field using EISCAT and IMP-8 data, *Ann. Geophys.*, *17*, 1306, https://doi.org/10.1007/s00585-999-1306-8.
- Kruparova, O., et al (2019). Statistical survey of the terrestrial bow shock observed by the Cluster spacecraft. *Journal of Geophysical Research: Space Physics*, *124*, 1539–1547. https://doi.org/10.1029/2018JA026272.
- Newell, P. T., et al. (2007), A nearly universal solar wind-magnetosphere coupling function inferred from 10 magnetospheric state variables. https://doi.org/10.1029/2006JA012015.
- Papitashvili, N. E., & King, J. H. (2020), OMNI 1-min Data [Data set], NASA Space Physics Data Facility, https://doi.org/10.48322/45bb-8792; Accessed on 14 May 2024.
- Shepherd, S. G *et al.*(2002) Cross polar cap potentials measured with Super Dual Auroral Radar Network during quasi-steady solar wind and interplanetary magnetic field conditions, *J. Geophys. Res.*, *107*(A7), https://doi.org/10.1029/2001JA000152.